SAND99-0751J

INVERSION OF HEAD WAVE TRAVELTIMES FOR THREE-DIMENSIONAL PLANAR STRUCTURE

David F. Aldridge[1] and Douglas W. Oldenburg[2]

[1] Geophysical Technology Department
Sandia National Laboratories
Albuquerque, New Mexico, USA, 87185-0750

Phone: 505-284-2823
Email: dfaldri@sandia.gov

[2] Department of Earth and Ocean Sciences
University of British Columbia
129-2219 Main Mall
Vancouver, British Columbia, Canada, V6T 1Z4

Phone: 604-822-2823
Email: doug@geop.ubc.ca

Abbreviated Title: **3D Planar Structure**

Submitted to *Geophysical Journal International*

March 1999

DISCLAIMER

SUMMARY

Inversion of head wave arrival times for three-dimensional (3D) planar structure is formulated as a constrained parameter optimization problem, and solved via linear programming techniques. The earth model is characterized by a set of homogeneous and isotropic layers bounded by plane, dipping interfaces. Each interface may possess arbitrary strike and dip. Predicted data consists of traveltimes of critically refracted waves formed on the plane interfaces of the model. The nonlinear inversion procedure is iterative; an initial estimate of the earth model is refined until an acceptable match is obtained between observed and predicted data. Inclusion of *a priori* constraint information, in the form of inequality relations satisfied by the model parameters, assists the algorithm in converging toward a realistic solution. Although the 3D earth model adopted for the inversion procedure is simple, the algorithm is quite useful in two particular contexts: (i) it can provide an initial model estimate suitable for subsequent improvement by more general techniques (i.e., traveltime tomography), and (ii) it is an effective analysis tool for investigating the power of areal recording geometries for detecting and resolving 3D dipping planar structure.

Key Words: Refraction seismology, traveltime, layered media, inversion.

INTRODUCTION

Head wave traveltimes are commonly analyzed and interpreted within the framework of one- or two-dimensional (1D or 2D) layered earth models. Extension of these techniques to three-dimensional (3D) layered media should provide more general tools for determining subsurface seismic properties. Critically or near-critically refracted arrivals are particularly valuable for inferring the seismic velocities of layered geologic media. Also, head waves often constitute first arrivals in many field experiments, and thus can be picked with greater accuracy than later arrivals.

Although numerous investigators have studied inversion of reflection traveltimes for 3D layered structure (e.g., Hubral 1976, Gjøystdal & Ursin 1981, Chiu *et al.* 1986, Chiu & Stewart 1987, Lin 1989, Phadke & Kanasewich 1990), the analogous situation for refraction traveltime data has not been thoroughly examined. Kanasewich and Chiu (1985) present a method for jointly inverting reflection and refraction traveltimes to determine 3D structure. Forward calculation of traveltimes is achieved with the iterative ray bending method of Chander (1977). Aldridge (1989) describes a method for recovering the attitude, velocity, and depth of a plane subsurface refractor from head wave arrivals recorded along two line profiles. However, the approach cannot be generalized to non-profile recording geometries. The present work allows an arbitrary distribution of sources and receivers on the surface.

This study describes an algorithm for inversion of head wave arrival times for 3D planar structure. The earth model is characterized by a stack of homogeneous and isotropic layers bounded by plane interfaces. Each interface may have arbitrary strike and dip. The inversion method is iterative; an initial estimate of the model parameters is refined until an acceptable match is obtained between observed and predicted data. Rapid forward modeling of head wave traveltimes and their partial derivatives is achieved with a combination of analytical and numerical techniques. The forward computation method does not entail iterative ray shooting or ray bending, which can be time consuming processes in 3D. A novel feature of the inversion procedure is the inclusion of constraint information in the form of inequality relations satisfied by the model parameters. Often, *a priori* geological or geophysical information is available to guide and constrain a non-linear traveltime inversion. This is particularly helpful for the inversion of head wave traveltimes, because the problem can be very ill-posed and admit numerous solutions.

The 3D layered earth model adopted for the inversion procedure is, admittedly, quite simple. Nevertheless, it can be an adequate representation of geophysical reality at various depth and lateral scales. This inversion approach is especially useful in two particular contexts: (i) it can provide an initial earth model estimate suitable for subsequent refinement by techniques that allow more general 3D variability in the parameters [e.g., reflection and/or refraction traveltime tomography (Hole 1992; Zelt *et*

al. 1996)], and (ii) it can be used as an analysis tool for investigating the capabilities of various recording geometries for detecting and resolving 3D dipping structure. These issues are facilitated by the extremely rapid execution speed of the algorithm.

After a discussion of the mathematical basis of the inversion technique, the algorithm is tested on both synthetic and field-acquired traveltime data. Inversion of refraction data from the Peace River Arch region of northwest Alberta and northeast British Columbia, Canada indicates that the algorithm can be a useful tool for analysis of head wave traveltimes recorded in a broadside configuration.

INVERSION MATHEMATICS

General theory

Let the observed arrival times for the experiment be organized into an I-dimensional column vector $\mathbf{t}_{obs}$. The earth model is characterized by a finite set of scalar parameters m_j, $j = 1,2,\ldots,J$. These are organized into an J-dimensional column vector $\mathbf{m}$. Predicted head wave traveltimes generated by this model are designated by the I-dimensional vector $\mathbf{t}_{prd}(\mathbf{m})$. Then, a first order Taylor series expansion of the observed data about the particular model $\mathbf{m}^n$ yields the expression

$$\mathbf{A}(\mathbf{m}^n)\Delta\mathbf{m}^{n+1} = \Delta\mathbf{t}(\mathbf{m}^n), \tag{1}$$

where $\Delta\mathbf{t}(\mathbf{m}^n) \equiv \mathbf{t}_{obs} - \mathbf{t}_{prd}(\mathbf{m}^n)$ is the *data discrepancy vector*, $\Delta\mathbf{m}^{n+1} \equiv \mathbf{m}^{n+1} - \mathbf{m}^n$ is the *parameter update vector*, and the elements of the $I \times J$ *sensitivity matrix* $\mathbf{A}(\mathbf{m}^n)$ are given by

$$\left[\mathbf{A}(\mathbf{m}^n)\right]_{ij} = \left.\frac{\partial t_i^{prd}}{\partial m_j}\right|_{\mathbf{m}=\mathbf{m}^n}. \tag{2}$$

In these and subsequent expressions, the superscript n is the iteration index.

In many crustal seismic reflection and refraction experiments, the system (1) is overdetermined, underconstrained, and inconsistent. A popular solution technique for $\Delta\mathbf{m}^{n+1}$ is the damped least squares method. The updated parameter vector is then obtained via $\mathbf{m}^{n+1} = \mathbf{m}^n + \Delta\mathbf{m}^{n+1}$. Iterations continue until an acceptable fit to the observed traveltime data is achieved. This strategy is termed "creeping" (Scales *et al.* 1990) because the final solution is obtained by the addition of (possibly many) small perturbations to an initial guess.

An alternative approach is used in this study to obtain the improved model parameter vector. Substituting the definition of the parameter update vector into (1) and rearranging terms gives

$$\mathbf{A}(\mathbf{m}^n)\mathbf{m}^{n+1} = \Delta\mathbf{t}(\mathbf{m}^n) + \mathbf{A}(\mathbf{m}^n)\mathbf{m}^n . \tag{3}$$

The right side of this expression consists of known quantities. Hence, equation (3) can be solved directly for the new model parameter vector $\mathbf{m}^{n+1}$. Scales *et al.* (1990) refer to this technique as "jumping" because, in the absence of additional constraints, the size of the model change between successive iterations $\|\mathbf{m}^{n+1} - \mathbf{m}^n\|$ is not restricted to be small. Moreover, since the inversion is formulated in terms of the model itself, rather than a model perturbation, the jumping strategy facilitates the incorporation of constraint information into the algorithm. In this work, constraints are mathematically expressed in the form of inequality relations satisfied by the model parameter vector:

$$\mathbf{m}^- \le \mathbf{m}^{n+1} \le \mathbf{m}^+ , \tag{4a}$$

where vectors $\mathbf{m}^-$ and $\mathbf{m}^+$ are lower and upper bounds on the model, respectively. These bounds arise from *a priori* geological or geophysical knowledge (or assumptions) about the earth model. For example, the model parameters in this study are strictly non-negative. Thus, if the lower bound is set equal to $\mathbf{0}$, negative values are excluded on each iteration of the inversion procedure. This is required for meaningful forward modeling of traveltimes. The inequality bounds in (4a) can also be used to severely restrict (or even eliminate) the variation of a certain parameter on successive iterations of the inversion. In this situation, upper and lower bounds are narrowly established about an accurately known (or preferred) value for the particular parameter.

The inversion algorithm can also be stabilized by limiting the size of the model change between iterations. Hence, if $\delta\mathbf{m}$ is a vector of upper bounds on the parameter increments, the updated parameter vector must satisfy the additional inequality constraints

$$\mathbf{m}^n - \delta\mathbf{m} \le \mathbf{m}^{n+1} \le \mathbf{m}^n + \delta\mathbf{m} . \tag{4b}$$

These constraints fulfill the same regularizing role as the damping parameter in a damped least squares solution of the original equation (1). If a reasonably good initial estimate $\mathbf{m}^0$ for the model is available, and if $\|\delta\mathbf{m}\|$ is sufficiently small, then the constraints (4b) assure that the algorithm iterates toward a solution in the neighborhood of $\mathbf{m}^0$, rather than jumping to a remote region of model space.

The linearized data equations (3) are usually inconsistent, i.e., an exact solution does not exist. Two reasons for this are (i) the observed traveltimes are contaminated with random picking errors, and (ii) the calculated traveltimes may have inadequate accuracy due to sparse and/or gross model parameterization. A robust solution to this inconsistent system can be obtained by minimizing the l_1 norm of the misfit. Linear programming provides a convenient solution method because the model parameters are intrinsically non-negative and are constrained by inequalities (4a,b). In order to pose the problem in the context of linear programming, an I-dimensional residual vector $\mathbf{r}$ is introduced into equation (3) as follows:

$$\mathbf{A}(\mathbf{m}^n)\mathbf{m}^{n+1} + \mathbf{r} = \Delta\mathbf{t}(\mathbf{m}^n) + \mathbf{A}(\mathbf{m}^n)\mathbf{m}^n . \tag{4c}$$

The elements of $\mathbf{r}$ constitute additional unknown variables that must be solved for. The problem now consists of determining the model parameter vector $\mathbf{m}^{n+1}$ and the residual vector $\mathbf{r}$ that simultaneously satisfy the inequality constraints (4a,b), the equality constraints (4c), and that minimize the l_1 norm of the residual

$$\|\mathbf{r}\|_1 = \sum_{i=1}^{I} |r_i| . \tag{4d}$$

A standard linear programming routine is used here to solve the constrained optimization problem specified by equations (4a,b,c,d). After an improved model parameter vector $\mathbf{m}^{n+1}$ is obtained, the l_1 norm of the misfit between observed and predicted traveltimes $\| \mathbf{t}_{obs} - \mathbf{t}_{prd}(\mathbf{m}^{n+1}) \|_1$ is computed. Iterations cease when this misfit reaches some acceptable level, or exhibits negligible change on successive iterations. The elements of the residual vector $\mathbf{r}$ play no further role after equations (4a,b,c,d) are solved, and are discarded. However, the l_1 norm of the residual (4d) is monitored on each iteration in order to assess how closely the linearized data equations have been fit.

Finally, the flexibility of the inversion algorithm is enhanced by including variable weighting of both the traveltime data and the model parameters. Equation (3) is modified to

$$\left[\mathbf{W}_d \mathbf{A}(\mathbf{m}^n)\mathbf{W}_p^{-1}\right]\left[\mathbf{W}_p \mathbf{m}^{n+1}\right] = \mathbf{W}_d \Delta\mathbf{t}(\mathbf{m}^n) + \left[\mathbf{W}_d \mathbf{A}(\mathbf{m}^n)\mathbf{W}_p^{-1}\right]\left[\mathbf{W}_p \mathbf{m}^n\right], \tag{5}$$

where $\mathbf{W}_d$ and $\mathbf{W}_p$ are data and parameter weighting matrices, respectively. Currently, these are restricted to be diagonal matrices. Thus, premultiplication of the sensitivity matrix by $\mathbf{W}_d$ corresponds to row weighting and postmultiplication by $\mathbf{W}^{-1}_p$ corresponds to column weighting.

The data weighting matrix can be used to emphasize those particular traveltimes judged to be more significant for the inversion. The parameter weighting matrix serves to nondimensionalize and normalize elements of the model parameter vector $\mathbf{m}^{n+1}$. This is a practical concern in inversion algorithms where the model is characterized by parameters with different physical dimensions and/or widely varying numerical magnitudes. The conditioning of the sensitivity matrix $\mathbf{A}(\mathbf{m}^n)$ is improved by column scaling by $\mathbf{W}^{-1}_p$. Thus, numerical roundoff error associated with the linear programming solution is reduced. Suitable units of measure are chosen for the various model parameters; the reciprocals of these scalars form the diagonal elements of $\mathbf{W}_p$. The inequality constraints (4a,b) on the model must also be nondimensionalized in the same manner. If the weighted parameter vector calculated by the inversion algorithm is designated $\mathbf{m}^{n+1}$, then the physical parameters required for forward modeling of traveltimes are obtained via $\mathbf{m}^{n+1} = \mathbf{W}^{-1}_p \mathbf{m}^{n+1}$.

Calculation of Traveltimes and Sensitivities

A simple 3D earth model consisting of a single layer overlying a halfspace is characterized by the five-element parameter vector $\mathbf{m} = [v_1, v_2, \phi, \theta, h]^T$, where v_1 and v_2 are P-wave velocities of the two media, ϕ and θ are interface orientation angles, and h is the vertical depth to the refractor below the coordinate origin. Aldridge (1989) derives a closed form expression for head wave traveltime in terms of these parameters. Hence, formulae for the elements of the sensitivity matrix can be obtained by straightforward partial differentiation. However, a substantial simplification arises by redefining the set of model parameters as $\mathbf{m} = [s_1, i_c, \phi, \theta, h]^T$ where $s_1 = 1/v_1$ is the layer slowness and $i_c = \sin^{-1}(v_1/v_2)$ is the critical refraction angle. In terms of these new parameters, head wave traveltime is

$$T = s_1 \sin(i_c - \delta)X + 2s_1 \cos i_c \left[h\cos\phi - (x_S \cos\theta + y_S \sin\theta)\sin\phi\right], \qquad (6)$$

where $\delta \equiv \sin^{-1}[\sin\phi \cos(\Psi-\theta)]$. Symbols x_S and y_S are the horizontal coordinates of the source, and X and Ψ are the offset and azimuth to the receiver, respectively. Note that equation (6) is a *linear* function of the layer slowness s_1. Differentiating (6) yields the traveltime sensitivities

$$\frac{\partial T}{\partial s_1} = \sin(i_c - \delta)X + 2\cos i_c\left[h\cos\phi - (x_S\cos\theta + y_S\sin\theta)\sin\phi\right], \tag{7a}$$

$$\frac{\partial T}{\partial i_c} = s_1\cos(i_c - \delta)X - 2s_1\sin i_c\left[h\cos\phi - (x_S\cos\theta + y_S\sin\theta)\sin\phi\right], \tag{7b}$$

$$\frac{\partial T}{\partial \phi} = \frac{-s_1\cos(i_c - \delta)\cos\phi\cos(\Psi - \theta)}{\cos\delta}X - 2s_1\cos i_c\left[h\sin\phi + (x_S\cos\theta + y_S\sin\theta)\cos\phi\right], \tag{7c}$$

$$\frac{\partial T}{\partial \theta} = \frac{-s_1\cos(i_c - \delta)\sin\phi\sin(\Psi - \theta)}{\cos\delta}X + 2s_1\cos i_c\sin\phi(x_S\sin\theta - y_S\cos\theta), \tag{7d}$$

$$\frac{\partial T}{\partial h} = 2s_1\cos i_c\cos\phi. \tag{7e}$$

The i^{th} row of the $I \times 5$ sensitivity matrix $\mathbf{A}(\mathbf{m}^n)$ is obtained by evaluating these relations with the current model vector $\mathbf{m}^n$ and with the geometric parameters $[x_{Si}, y_{Si}, X_i, \Psi_i]$ appropriate for the i^{th} recorded traveltime. The number of traveltimes usually exceeds 5, and thus the matrix is overdetermined. However, in some situations, the matrix is also rank deficient. If the refracting horizon is horizontal (i.e., $\phi = 0$) then the derivative $\partial T/\partial\theta$ vanishes, and the fourth column of the sensitivity matrix is identically zero. This will occur, for example, if a 1D earth model is used for the initial parameter vector estimate.

Calculation of head wave traveltime sensitivities for a multilayered earth model is more complicated because a closed form mathematical expression for the arrival time does not exist. However, Aldridge (1992, 1999) gives a head wave traveltime formula for this situation that can be evaluated with minimal numerical effort. A combination of analytical and numerical techniques can then be used to calculate the sensitivities. In this study, sources and receivers are restricted to the horizontal surface. Thus, if there are K interfaces in the earth model, then there are total of $J = 4K$-3 model parameters (K layer slownessess, $2K$-2 interface orientation angles, and K-1 layer thicknesses). These parameters are organized into the J-dimensional column vector

$$\mathbf{m} = \left[s_1 \ldots s_K, \phi_2 \ldots \phi_K, \theta_2 \ldots \theta_K, h_1 \ldots h_{K-1}\right]^T,$$

where s_j is a layer slowness, ϕ_j is an interface dip angle, θ_j is an interface azimuth angle, and h_j is a vertical layer thickness measured at the coordinate origin. Interfaces are numbered sequentially from the surface (interface 1) in the downward direction. Interface j overlies layer j.

A "slope and intercept" expression for the traveltime of a head wave critically refracted on interface k ($2 \le k \le K$) of a multilayered earth model is derived by Aldridge (1992, 1999):

$$T_k(x_S, y_S, X, \Psi) = m_k(\Psi) X + b_k(x_S, y_S, \Psi), \tag{8}$$

where, as above, x_S and y_S are the horizontal coordinates of the source (on the surface), X is the source-receiver offset distance, and Ψ is the source-to-receiver azimuth angle. The slope $m_k(\Psi)$ and intercept $b_k(x_S, y_S, \Psi)$ are

$$m_k(\Psi) = s_1 \left[\cos\Psi \, q_{1k,x} + \sin\Psi \, q_{1k,y} \right], \tag{9a}$$

and

$$b_k(x_S, y_S, \Psi) = \sum_{j=1}^{k-1} s_j h_j (p_{jk,z} - q_{jk,z}) - s_1 \left[x_S (p_{1k,x} - q_{1k,x}) + y_S (p_{1k,y} - q_{1k,y}) \right]. \tag{9b}$$

Expressions (9a,b) contain the components of two sets of unit vectors $\mathbf{p}_{jk}$ and $\mathbf{q}_{jk}$ that describe the propagation directions within layer j of a wave critically refracted on subsurface interface k:

$$\mathbf{p}_{jk} = p_{jk,x}\mathbf{i} + p_{jk,y}\mathbf{j} + p_{jk,z}\mathbf{k}, \qquad \mathbf{q}_{jk} = q_{jk,x}\mathbf{i} + q_{jk,y}\mathbf{j} + q_{jk,z}\mathbf{k},$$

with $||\mathbf{p}_{jk}||_2 = ||\mathbf{q}_{jk}||_2 = 1$. Vectors $\mathbf{p}_{jk}$ and $\mathbf{q}_{jk}$ (j=1,2,...,k-1) refer to the downward and upward propagating portions of the total raypath, respectively. The propagation direction along the critically refracting horizon is $\mathbf{p}_{kk} = \mathbf{q}_{kk}$. Equations (8) and (9a,b) are not "closed form" expressions for head wave traveltime because these unit propagation vectors depend implicitly on both the model $\mathbf{m}$ and the source-to-receiver recording azimuth Ψ. Nevertheless, if $\mathbf{m}$ and Ψ are specified, then all of the propagation vectors can be accurately computed, and the traveltime formula (8) can be numerically evaluated. The computation procedure does not involve any iterative 3D ray tracing (shooting or bending), and thus is extremely rapid.

Many of the elements of the sensitivity matrix $\mathbf{A}(\mathbf{m})$ can be determined by analysis. The traveltime of a head wave formed on interface k does not depend on parameters s_j, ϕ_j, and θ_j for $j > k$, or on h_j for $j \geq k$. Hence, these traveltime derivatives are identically zero. Moreover, the sensitivity to layer thickness h_j for $j < k$ is derived directly from the above expression for intercept time: $\partial T_k / \partial h_j = s_j \, (p_{jk,z} - q_{jk,z})$. The remaining sensitivities must be evaluated by a finite-difference technique. Let $\mathbf{dm}_j$ be a model perturbation vector with zeros in all element positions except the j^{th}. Then, the partial derivative of head wave traveltime with respect to parameter m_j is approximated by the forward finite-difference

$$\frac{\partial T_k}{\partial m_j} \approx \frac{T_k(\mathbf{m} + \mathbf{dm}_j) - T_k(\mathbf{m})}{\left\| \mathbf{dm}_j \right\|_2}. \tag{10}$$

Unit propagation vectors are generated for both the perturbed model $\mathbf{m} + \mathbf{dm}_j$ and the unperturbed model $\mathbf{m}$. These are then used in formulae (8) above to calculate traveltimes for each model. Finally, substituting these traveltimes into (10) yields an approximation for the required derivative. The size of the model perturbation $\|\mathbf{dm}_j\|_2$ is typically about 1% of the value of the associated model parameter. Although a centered finite-difference scheme would yield greater accuracy, the one-sided approximation adopted here requires less computational effort. Only two traveltime computations are needed for each model parameter, instead of three.

SYNTHETIC DATA EXAMPLES

The two examples discussed in this section are representative of a large number of computational experiments conducted with the inversion algorithm. Both the single-layer and multiple-layer variants of the algorithm are examined. The first example demonstrates that the single-layer version is capable of returning the correct solution under a variety of operating conditions. However, as indicated in the second example, the multilayer version appears to require fairly restrictive constraints in order to iterate toward the correct model.

Single Layer

The earth model used for the first example consists of a single layer overlying a halfspace and is defined by the parameters

$v_1 = 1500\,\text{m/s}, \qquad v_2 = 2500\,\text{m/s}, \qquad \phi = 5°, \qquad \theta = 45°, \qquad h = 100\,\text{m}.$

Critically refracted arrival times for two areal recording geometries are generated from equation (6). Inversions are performed with both accurate and error-contaminated traveltimes.

Figure 1a is a plan view of a triangular data acquisition geometry. Thirty receivers are deployed around the perimeter of an equilateral triangle with sides 500 m long. Each side contains 11 receivers separated by 50 m. All receivers record energy from sources that are activated sequentially at the three vertices of the triangle. However, some source-receiver offsets are less that the critical offset distance, and thus these receivers do not detect a head wave arrival. These fictitious times are excluded from the inversions. A total of $I = 73$ uniformly weighted traveltimes are used to recover the $J = 5$ earth model parameters.

Numerical results from a few typical inversion runs are described here. The iterative inversion procedure is initiated with a 1D model given by

$v_1 = 1000\,\text{m/s}, \qquad v_2 = 2000\,\text{m/s}, \qquad \phi = 0°, \qquad \theta = 0°, \qquad h = 85\,\text{m}.$

After eight iterations, the exact (i.e., within one significant digit) earth model parameters are returned. The initial traveltime misfit of 79.6 ms is reduced to 0.1 ms; iterations terminate when the relative change in misfit is less than 1%. A wide variety of starting models yields essentially the same final solution, although the number of iterations required for convergence varies. Also, the inversion is stable when the traveltimes are contaminated with small random errors. Random numbers drawn from a uniform probability distribution on ±4 ms are added to the accurate times, and the algorithm is initiated with the same starting model. After five iterations, the following solution is obtained:

$v_1 = 1497\,\text{m/s}, \qquad v_2 = 2549\,\text{m/s}, \qquad \phi = 5°, \qquad \theta = 52°, \qquad h = 100\,\text{m}.$

Iterations cease when the misfit decreases below 2.3 ms, equal to one standard deviation of the noise. Note that the overburden velocity v_1 has been correctly estimated from the refraction data alone! This interesting (and unusual) result is consistent with a theoretical analysis by Aldridge (1992).

These results suggest that the triangular recording array is a useful configuration for determining 3D planar structure. This particular geometry combines an adequate distribution of offset and azimuth together with three reciprocal time pairs. These are favorable attributes for a successful inversion of refraction arrival times via the time term, delay time, and reciprocal time inversion methods. The triangle

was first investigated by Gardner (1939) who demonstrated that it yields an exact solution for the delay times at the three vertices. More recently, the triangular array has been used for deep crustal seismic exploration in Saskatchewan (Kanasewich & Chiu 1985) and British Columbia (Zelt *et al.* 1996).

Other recording geometries are considerably less robust in detecting and resolving 3D dipping structure. Figure 1b depicts two parallel line arrays, separated by 200 m, oriented along the strike direction of the subsurface refractor (NW-SE). Each spread contains 11 geophones (receiver interval = 50 m) that record head wave arrivals from a source located at the center of the opposing array. This broadside recording pattern simulates aspects of the "swath geometry" commonly used for 3D seismic reflection surveys. Using the same starting model, inversion of the 22 equi-weighted broadside traveltimes yields

$$v_1 = 1286\,\text{m/s}, \qquad v_2 = 2500\,\text{m/s}, \qquad \phi = 5^\circ, \qquad \theta = 45^\circ, \qquad h = 80\,\text{m}.$$

The initial traveltime misfit of 66.4 ms is reduced to near zero in eight iterations. Although this model generates an exact fit to the data, the overburden velocity v_1 and the vertical depth h are incorrect. A similar effect is observed when the inversion is initiated from numerous different starting models. This situation illustrates the classical tradeoff between overburden velocity and refractor depth in seismic refraction interpretation. If additional *a priori* data are introduced into the inverse problem, then a correct solution is possible. For example, the interface depth may be known from a borehole drilled at the coordinate origin. Constraining the depth to satisfy $99\,\text{m} < h < 101\,\text{m}$ yields the model

$$v_1 = 1490\,\text{m/s}, \qquad v_2 = 2500\,\text{m/s}, \qquad \phi = 5^\circ, \qquad \theta = 45^\circ, \qquad h = 99\,\text{m},$$

which is substantially correct. Alternately, constraining the overburden velocity with the inequalities $1450\,\text{m/s} < v_1 < 1550\,\text{m/s}$ yields the erroneous 1D model

$$v_1 = 1450\,\text{m/s}, \qquad v_2 = 2494\,\text{m/s}, \qquad \phi = 0^\circ, \qquad \theta = 0^\circ, \qquad h = 94\,\text{m}.$$

Evidently, the broadside geometry illustrated in Figure 1b allows many solutions to this nonlinear inverse problem. However, if the both the inline and broadside head wave arrivals recorded on each spread are included in the inversion (so now $I = 32$), the correct model is recovered in seven iterations. Head waves recorded along strike provide excellent control on the velocity of the refracting medium. Aldridge (1989) demonstrates that the measured apparent velocity equals the true velocity in this situation. As expected,

the inversion degrades when the exact traveltimes are contaminated with uniformly distributed random errors on ±4 ms. The model

$$v_1 = 1559\,\text{m/s}, \qquad v_2 = 2664\,\text{m/s}, \qquad \phi = 5^\circ, \qquad \theta = 43^\circ, \qquad h = 107\,\text{m},$$

is obtained in seven iterations with a traveltime misfit of 2.4 ms.

Multiple Layers

The earth model used for the second example consists of two layers overlying a halfspace and is defined by the parameters

$$\begin{aligned} v_1 &= 1500\,\text{m/s}, & \phi_1 &= 0^\circ, & \theta_1 &= 0^\circ, & z_1 &= 0\,\text{m}, \\ v_2 &= 2000\,\text{m/s}, & \phi_2 &= 3^\circ, & \theta_2 &= 180^\circ, & z_2 &= 40\,\text{m}, \\ v_3 &= 2500\,\text{m/s}, & \phi_3 &= 5^\circ, & \theta_3 &= 45^\circ, & z_3 &= 100\,\text{m}. \end{aligned}$$

Model parameters ϕ_1, θ_1, and z_1 are not allowed to vary in the inversion. Hence, there are only $J = 9$ parameters to estimate. Head wave traveltimes for each critically refracting horizon are generated by evaluating equation (8). The recording geometry used is the triangular array displayed in Figure 1a. Also, precritical offset arrivals are included in the traveltime dataset (in an actual field experiment, these times could be obtained by extrapolation or phantoming). Hence, there are a total of $I = 174$ uniformly weighted arrival times input to the inversion procedure.

If restrictive constraints are imposed on the model parameters, then it is possible to recover the correct solution with the multilayer algorithm. For example, constraining the velocity v_1 and the depth z_2 equal to the true values allows the algorithm to iterate to the known solution from a 1D starting model. Also, if narrow bounds are established on the velocities and depths (±50 m/s and ±5 m about the true values, respectively) then the correct solution is obtained from a nearby initial model. However, a relatively unconstrained inversion invariably yields an erroneous result for this simulated experiment. It is probable that the objective function (4d), which only measures the misfit of the linearized data equations, has many local minima that preclude convergence to the desired global minimum.

FIELD DATA EXAMPLE

Deep seismic refraction data were acquired in the Peace River Arch (PRA) region of northwest Alberta and northeast British Columbia, Canada in 1985. In addition to four inline profiles, two broadside profiles were recorded. Figure 2 illustrates the source-receiver geometry for these two profiles. Shot A4 in the west is recorded by the north-south trending line A, and shot B4 in the north is recorded by the east-west trending line B. Offset distances range from 249-313 km on line A, and from 262-344 km on line B. Each receiver array subtends an azimuthal angle of ~64° relative to its source. The first arrivals at the recording sites are interpreted to be waves that are critically or near-critically refracted at the Moho. Hence, inversion of the first break traveltimes can provide an estimate of the regional depth and dip of the Moho beneath the Peace River Arch.

In this example, the broadside arrival times are inverted within the framework of a simple "layer over a halfspace" earth model. No attempt is made to infer a detailed structural picture of the crust and Moho in the PRA region. Rather, the intent is to recover a large scale 3D model that can be subsequently refined by other traveltime interpretation/inversion methods. Initial estimates of the model parameters are obtained from crustal sections along lines A and B given by Zelt & Ellis (1989). These sections were derived by interpreting the inline refraction data of the PRA experiment via a trial-and-error forward modeling approach.

There are 83 first break picks from line A and 52 first break picks from line B. Thus, $I = 135$ equally weighted traveltimes are input to the iterative inversion procedure. The first arrivals recorded at these long offset distances are emergent, and the estimated picking error is ±50 ms.

The effect of variable near surface structure on the head wave arrival times can be reduced by applying static corrections to the picked first breaks. Static corrections are commonly applied to seismic reflection data for this same purpose. However, there is an important distinction between the corrections for the two types of data. In the refraction case, the static is designed to remove the *refraction delay time* influence of the near surface structure, and then replace it with the delay time contribution of a constant velocity medium. In the reflection case, the correction pertains to the *vertical traveltime* through the actual and replacement media. Statics application is an important preprocessing step for the PRA broadside data because the subsequent inversion assumes a very simple earth model. In effect, an attempt is made to "make the data fit the model" more closely. The refraction statics development in Appendix A assumes that near surface velocity information is available. For the PRA experiment, this is obtained from well log data along the two profile lines.

Inversion Results

The initial estimates of the earth model parameters are:

$$v_1 = 6.5\,\text{km/s}, \qquad v_2 = 8.25\,\text{km/s}, \qquad \phi = 2°, \qquad \theta = 270°, \qquad h = 40\,\text{km}.$$

Lower and upper parameter bounds are also inferred from the crustal sections in Zelt & Ellis (1989):

$$v_1^- = 6.0\,\text{km/s}, \qquad v_2^- = 7.5\,\text{km/s}, \qquad \phi^- = 0°, \qquad \theta^- = 0°, \qquad h^- = 38\,\text{km},$$
$$v_1^+ = 7.5\,\text{km/s}, \qquad v_2^+ = 8.5\,\text{km/s}, \qquad \phi^+ = 15°, \qquad \theta^+ = 360°, \qquad h^+ = 42\,\text{km}.$$

The bounds on the velocities must be transformed to equivalent bounds on the parameters s_1 (slowness) and i_c (critical angle) that are used by the inversion algorithm. After five iterations, the following model is returned:

$$v_1 = 6.21\,\text{km/s}, \qquad v_2 = 8.50\,\text{km/s}, \qquad \phi = 2.8°, \qquad \theta = 300.0°, \qquad h = 42\,\text{km}.$$

The initial traveltime misfit of 658 ms is reduced to 172 ms; iterations cease when the relative change in the misfit is less than 1%. Velocities v_1 and v_2 of this solution differ from the replacement and critical velocities (v_r and v_c, respectively) used for calculating refraction static corrections. Hence, the statics are recomputed with v_r = 6.2 km/s and v_c = 8.5 km/s (see Appendix A) and applied again to the picked arrival times. Then, initiating the inversion algorithm with the same starting model yields

$$v_1 = 6.17\,\text{km/s}, \qquad v_2 = 8.50\,\text{km/s}, \qquad \phi = 2.7°, \qquad \theta = 300.9°, \qquad h = 42\,\text{km},$$

in five iterations with a misfit of 171 ms. Although this model is not significantly different from the previous one, it is consistent with the assumptions used for calculating the statics.

A comparison between the observed arrival times (after application of static corrections) and the traveltimes predicted by the model produced by the inversion is displayed in Figure 3. Evidently, the simple five-parameter earth model provides an adequate explanation for the gross character of the broadside arrival time curves. Small scale variations in the predicted times (solid curves) are due strictly to recording geometry irregularities, rather than any subsurface structural complications. However, a large component of the total traveltime misfit must be attributed to structure or velocity variations that are

not modeled in the inversion procedure. This misfit is too large to be accounted for by random picking errors alone. For example, the predicted times are systematically greater than the observed times throughout the central portion of line B. This suggests that the Moho north of line B is not adequately represented by a plane interface bounded by uniform velocities.

Vertical depths to the Moho calculated from the inversion results are posted on a plan view of the PRA recording geometry in Figure 4. A depth trend is readily apparent, although the depth at the southern end of line A is probably too large. Southeastward dip of the Moho is suggested by interpretations of the inline refraction data on lines A and B, but not on the other lines of the PRA experiment (Zelt & Ellis 1989). Also, the velocities recovered by the 3D inversion are broadly consistent with those obtained previously. Of course, precise agreement cannot be expected. The mean crustal velocity is lower (6.17 km/s *vs.* ~6.6 km/s) and the sub-Moho velocity is higher (8.5 km/s *vs.* ~8.2 km/s). However, Zelt & Ellis (1989) infer a P_n velocity of 8.4 km/s along the northern half of line A and eastern quarter of line B.

Two-Dimensional Analysis

An independent check on the validity of the 3D inversion is provided by a simple 2D analysis technique. Assuming a 2D "layer over a halfspace" earth model, each arrival time recorded along a broadside profile can be individually inverted for an estimate of Moho depth beneath the associated receiver site. A depth profile for the Moho is constructed by plotting these depth estimates side-by-side. In the 2D case, head wave traveltime is

$$T(x_S, X) = \frac{\sin(i_c + \varphi)}{v_1} X + \frac{2h(x_S)\cos\varphi\cos i_c}{v_1}, \tag{11}$$

where $i_c = \sin^{-1}(v_1/v_2)$ is the critical angle and $h(x_S)$ is the vertical thickness of the layer at the source location. The interface dip angle φ may be positive, zero, or negative. This relation is rewritten as a quadratic form in $\cos\varphi$:

$$A\cos^2\varphi + B\cos\varphi + C = 0. \tag{12}$$

The three coefficients depend on earth model parameters [v_1, v_2, $h(x_S)$] and measured data [X, T] as follows:

$$A = 1 + \frac{4h(x_S)\cos i_c}{X}\left[\sin i_c + \frac{h(x_S)}{X}\cos i_c\right], \tag{13a}$$

$$B = -2\left[\frac{v_1 T}{X}\right]\left[\sin i_c + \frac{2h(x_S)}{X}\cos i_c\right],. \tag{13b}$$

$$C = \left[\frac{v_1 T}{X}\right]^2 - \cos^2 i_c . \tag{13c}$$

If values for v_1, v_2, and $h(x_S)$ are known (or assumed), then these coefficients can be evaluated numerically. Solution of equation (12) for $\cos\varphi$ is via the quadratic formula:

$$\cos\varphi = \frac{-B + \sqrt{B^2 - 4AC}}{2A}, \tag{14}$$

where the positive root is chosen by analyzing the form of the right side as $X \to +\infty$. There is still a two-fold ambiguity in determining the dip angle φ from its cosine. This is easily resolved by ensuring that the traveltime predicted by formula (11) agrees with the picked traveltime. Finally, once the dip angle is determined, the vertical depth to the refractor at any inline position x can be calculated via $h(x) = h(x_S) + (x\text{-}x_S)\tan\varphi$.

Figure 5 compares Moho depths calculated via the above method with those inferred from the parameters recovered by the 3D inversion. Vertical depths beneath the recording stations along each line are plotted. The coefficients in the quadratic (12) are evaluated with the parameters obtained from the 3D inversion procedure (v_1 = 6.17 km/s, v_2 = 8.50 km/s, $h(x_S)$ = 37.6 km for shot A4, and $h(x_S)$ = 34.8 km for shot B4). Short wavelength variations in the computed curves are artifacts of traveltime picking errors and/or small scale structural heterogeneity, and should be ignored. There is close agreement in the Moho depth trend calculated by these two completely different techniques, especially along line A. The larger departure of the two depth curves along line B suggests structural complexity north of this line in the Peace River Arch region.

Although the 2D inversion method is simple and appears to yield reasonable depth estimates, it requires assumptions of numerical values for three unknown model parameters [$v_1, v_2, h(x_S)$]. In contrast, the 3D inversion technique yields simultaneous estimates of all relevant earth model parameters.

Moreover, since it accomplishes a joint inversion of all of the error-contaminated traveltime data, it is more robust than the 2D method.

CONCLUSION

Inversion of head wave arrival times for 3D planar structure is formulated as a constrained parameter optimization problem, and solved via linear programming. The iterative inversion algorithm described here has the ability to converge to a realistic solution provided that (i) the data acquisition geometry is adequate, and (ii) sufficient *a priori* constraints are available. However, precise definitions of "adequate" and "sufficient" in this context are not known. Nevertheless, the inversion procedure provides a useful tool for examining these phenomena. In particular, the single layer variant of the algorithm can be used as an aid in designing areal recording geometries for detecting and resolving 3D dipping structure. Also, investigation of both synthetic and field recorded datasets indicates that it can be successfully applied to the inversion of broadside refraction data. There are relatively few techniques for effective interpretation of such data. Although the multiple layer version of the algorithm exhibits a greater tendency to converge to an erroneous result, several successful inversions have been achieved with the inclusion of sufficient constraints. *A priori* constraint information may arise from a variety of geological, geophysical, and/or engineering sources. Generalization of these algorithms to true 3D recording geometries (i.e., subsurface, as well as surface, sources and receivers) would be a useful extension. Moreover, in this situation, well log information regarding interface depths and layer velocities would supply the necessary constraint information.

ACKNOWLEDGMENTS

This research was conducted while the first author was a graduate student in the Department of Geophysics and Astronomy at the University of British Columbia. Support was provided by operating grant 5-84270 from the Natural Sciences and Engineering Research Council of Canada (principal investigator: Professor Douglas W. Oldenburg) and a Killam Predoctoral Fellowship from the University of British Columbia. Dr. Colin A. Zelt, currently with the Department of Geology and Geophysics at Rice University, performed the difficult task of picking traveltimes of emergent first arrivals recorded on the Peace River Arch broadside arrays. Sandia National Laboratories, a multiprogram science and engineering laboratory operated by the US Department of Energy under contract DE-AC04-94AL85000, is acknowledged for providing resources necessary for publishing this material.

REFERENCES

Aldridge, D.F., 1989. Attitude, velocity, and depth of a plane refractor from two line profiles, *Geophysics*, **54**, 1199-1203.

Aldridge, D.F., 1992. Analysis and inversion of seismic refraction traveltimes, *PhD. thesis*, University of British Columbia.

Aldridge, D.F., 1999. Head wave traveltimes in a three-dimensional multilayered earth, *Geophys. J. Int.*, submitted.

Chander, R., 1977. On tracing seismic rays with specified end points in layers of constant velocity and plane interfaces, *Geophys. Prosp.*, **25**, 120-124.

Chiu, S.K.L., Kanasewich, E.R. & Phadke, S., 1986. Three-dimensional determination of structure and velocity by seismic tomography, *Geophysics*, **51**, 1559-1571.

Chiu, S.K.L. & Stewart, R.R., 1987. Tomographic determination of three-dimensional seismic velocity and structure using well logs, vertical seismic profiles, and surface seismic data, *Geophysics*, **52**, 1085-1098.

Gardner, L.W., 1939. An areal plan of mapping subsurface structure by refraction shooting, *Geophysics*, **4**, 247-259.

Gjøystdal, H. & Ursin, B., 1981. Inversion of reflection times in three dimensions, *Geophysics*, **46**, 972-983.

Hole, J.A., 1992. Nonlinear high-resolution three-dimensional seismic travel time tomography, *J. Geophys. Res.*, **97**, 6553-6562.

Hubral, P., 1976. Interval velocities from surface measurements in the three-dimensional plane layer case, *Geophysics*, **41**, 233-242.

Kanasewich, E.R. & Chiu, S.K.L., 1985. Least-squares inversion of spatial seismic refraction data, *Bull. Seism. Soc. Am.*, **75**, 865-880.

Lin, T., 1989. Prestack traveltime inversion for three-dimensional structure, *Geophysics*, **54**, 359-367.

Phadke, S. & Kanasewich, E.R., 1990. Seismic tomography to obtain velocity gradients and three-dimensional structure and its application to reflection data on Vancouver Island, *Can. J. Earth Sci.*, **27**, 104-116.

Scales, J.A., Docherty, P. & Gersztenkorn, A., 1990. Regularisation of nonlinear inverse problems: imaging the near-surface weathering layer, *Inverse Problems*, **6**, 115-131.

York, D., 1966. Least-squares fitting of a straight line, *Can. J. Physics*, **44**, 1079-1086.

Zelt, B.C., Ellis, R.M., Clowes, R.M. & Hole, J.A., 1996. Inversion of three-dimensional wide-angle seismic data from the southwestern Canadian Cordillera, *J. Geophys. Res.*, **101**, 8503-8529.

Zelt, C.A., 1989. Seismic structure of the crust and upper mantle in the Peace River Arch region: *PhD. thesis*, University of British Columbia.

Zelt, C.A. & Ellis, R.M., 1989. Seismic structure of the crust and upper mantle in the Peace River Arch region, Canada, *J. Geophys. Res.*, **94**, 5729-5744.

LIST OF FIGURE CAPTIONS

Figure 1. Plan views of two areal recording arrays. Sources are indicated by asterisks and receivers by small crosses. (a) Triangular geometry. (b) Swath geometry. The strike and dip symbol in the upper right corner of each panel refers to a subsurface interface located 100 m below the coordinate origin (large cross).

Figure 2. Broadside recording geometry for the Peace River Arch seismic experiment. Sources are indicated by asterisks and receivers by small crosses.

Figure 3. Comparison between predicted traveltimes (solid lines) and observed traveltimes (triangles) on broadside lines A and B of the PRA experiment. Inline distance increases from north to south along line A, and from west to east along line B.

Figure 4. Vertical depths (in kilometers) to the Moho in the Peace River Arch region of northern Alberta inferred from 3D inversion results.

Figure 5. Comparison of vertical depths to the Moho beneath the receivers of lines A and B calculated by two different methods. Smooth curves in each panel are depths inferred from the 3D inversion results. Jagged curves are obtained from a simple 2D inversion method.

Figure A1. Receiver static functions for lines A and B of the PRA experiment. Squares refer to well locations where near surface velocity logs are available. Inline distance increases from north to south along line A, and from west to east along line B. (a) Statics calculated with v_c = 8.25 km/s and v_r = 6.6 km/s. (b) Statics calculated with v_c = 8.5 km/s and v_r = 6.2 km/s. v_c and v_r are critical refractor and replacement velocities, respectively.

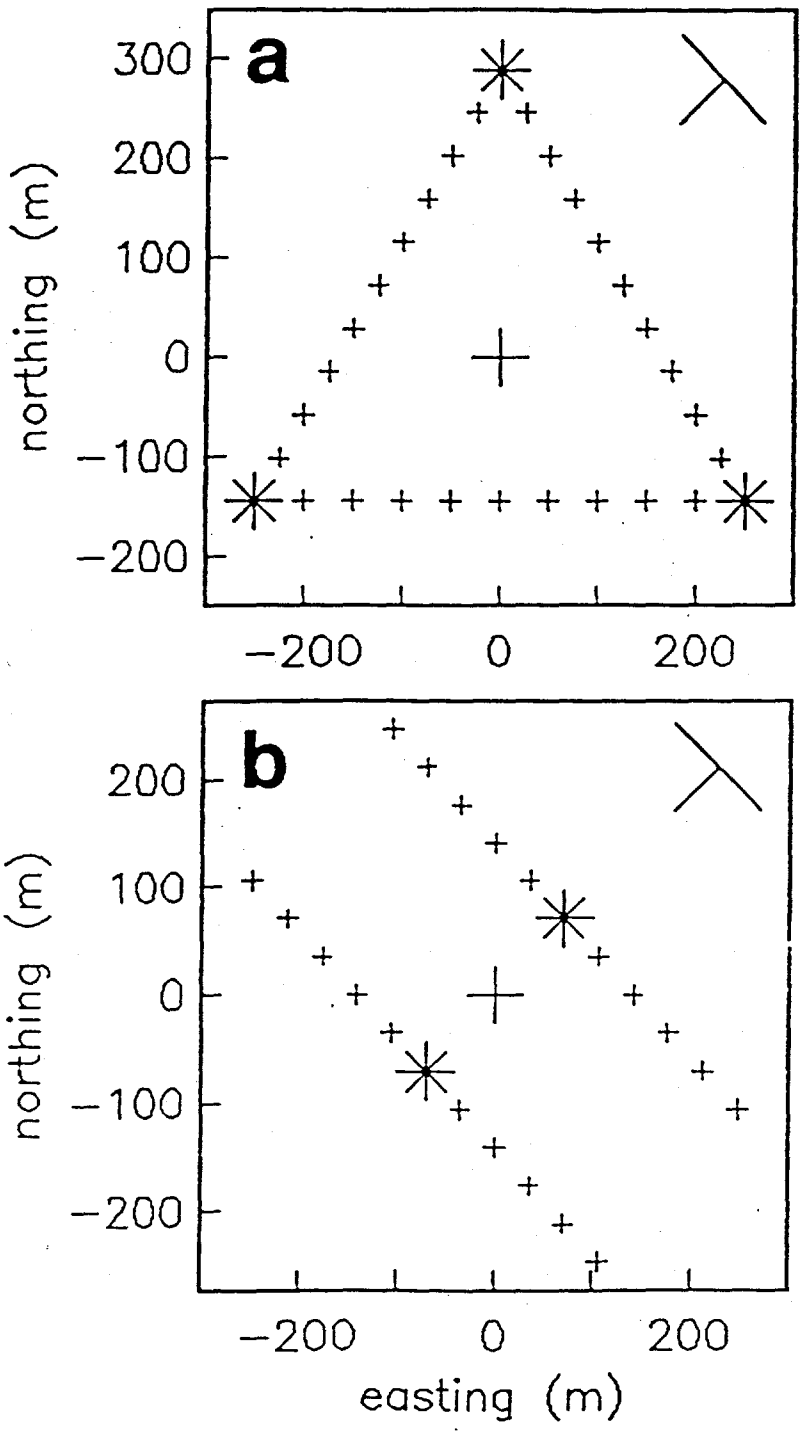
a
300
200
100
0
−100
−200
northing (m)
−200
0
200
b
200
100
0
−100
−200
northing (m)
−200
0
200
easting (m)

Fig. 1

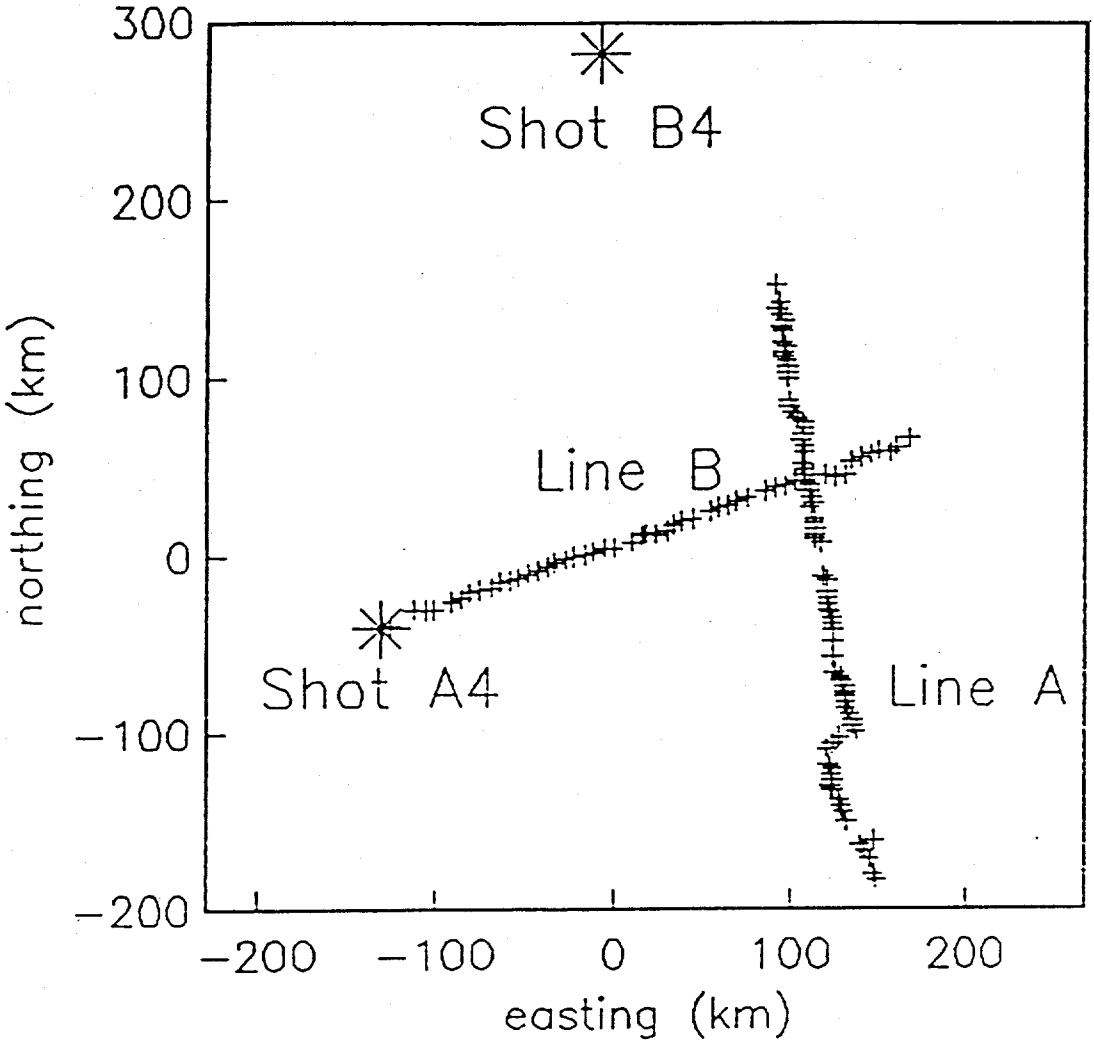
300
200
100
0
−100
−200
northing (km)
Shot B4
Line B
Shot A4
Line A
−200
−100
0
100
200
easting (km)

Fig. 2

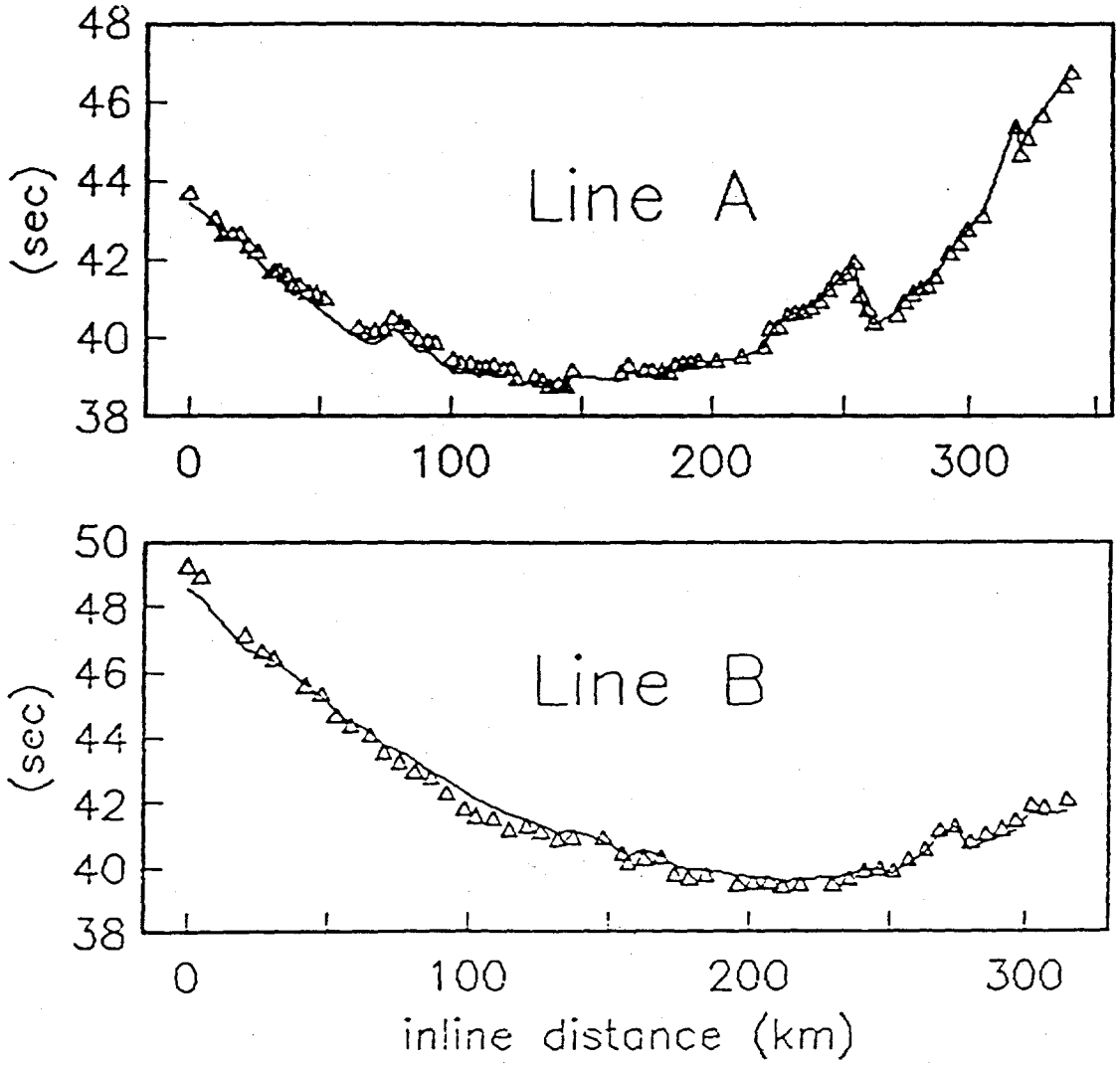
Line A
(sec)
48
46
44
42
40
38
0
100
200
300
Line B
(sec)
50
48
46
44
42
40
38
0
100
200
300
inline distance (km)

Fig 3

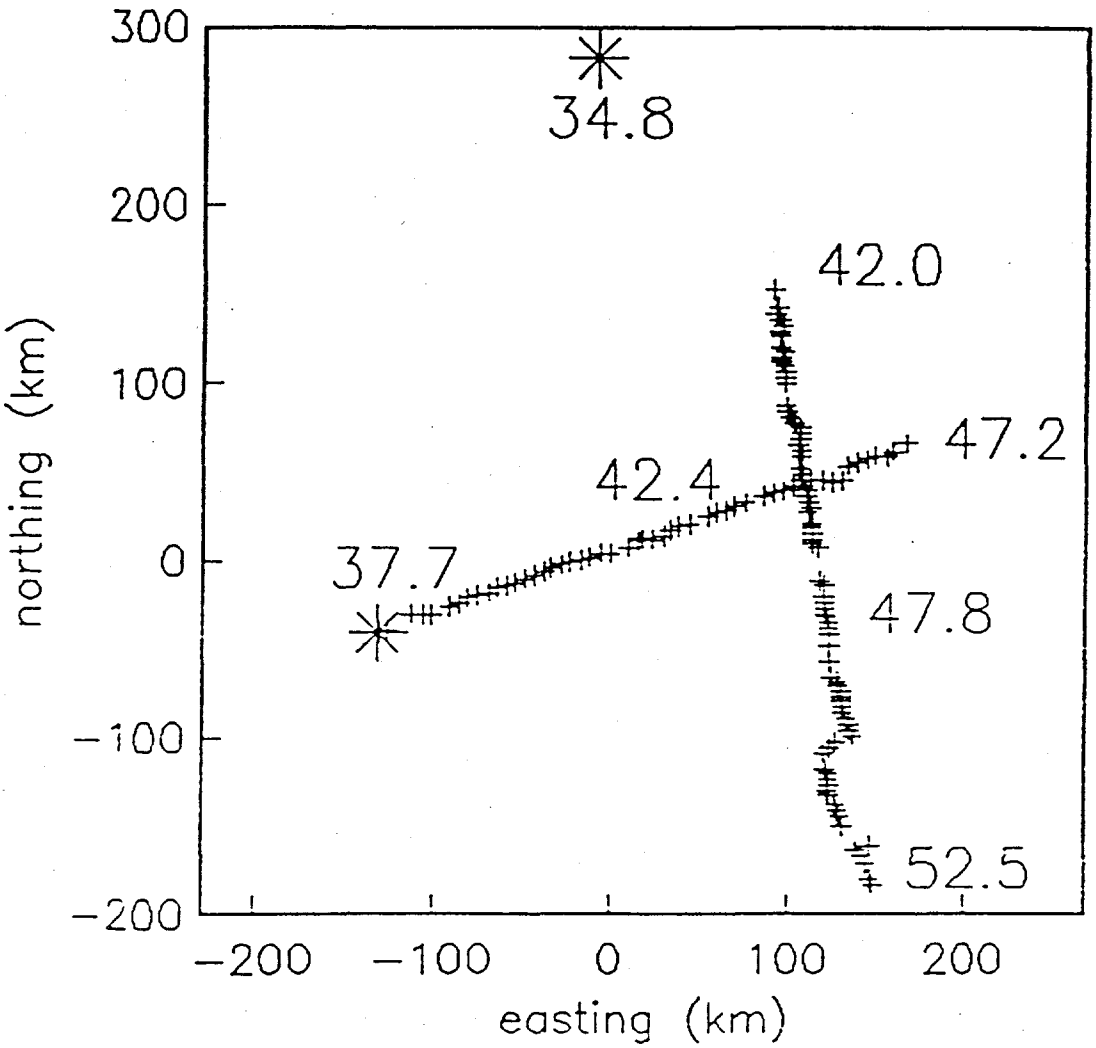
300
200
100
0
−100
−200
northing (km)
−200
−100
0
100
200
easting (km)
34.8
42.0
47.2
42.4
37.7
47.8
52.5

Fig. 4

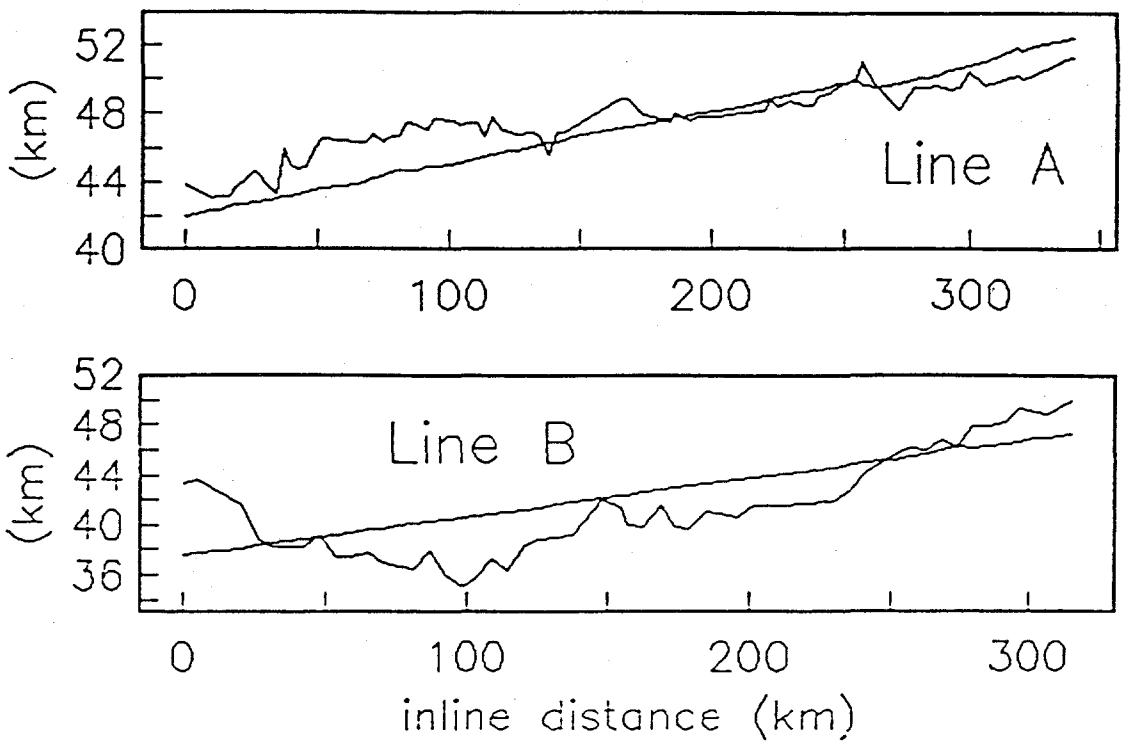
52
48
44
40
(km)
Line A
0
100
200
300
52
48
44
40
36
(km)
Line B
0
100
200
300
inline distance (km)

Fig. 5

APPENDIX A: REFRACTION STATIC CORRECTIONS

An expression for the static correction at each receiver site is derived by approximating the local near-surface velocity structure by a 1D stack of layers. The i^{th} layer is bounded from above and below by plane, horizontal interfaces at depths z_i and z_{i+1}, respectively. The P-wave velocity of the layer depends linearly on depth z and is given by $v_i(z) = v_i(0) + a_i z$. In this situation, the raypath associated with a particular ray parameter p is a circular arc. The upward propagation time across the layer is

$$\Delta t_i(p) = \frac{1}{a_i}\left[\cosh^{-1}\left(\frac{1}{pv_i}\right) - \cosh^{-1}\left(\frac{1}{pv_i'}\right)\right], \tag{A1}$$

where $v_i \equiv v_i(z_i)$ and $v_i' \equiv v_i(z_{i+1})$. Symbols v_i and v_i' denote the velocities at the top and bottom of the i^{th} layer, respectively. The horizontal distance accumulated by the wave as it traverses layer i is

$$\Delta x_i(p) = \frac{1}{pa_i}\left[\sqrt{1-(pv_i)^2} - \sqrt{1-(pv_i')^2}\right]. \tag{A2}$$

If the wave is critically refracted on a horizontal interface at greater depth, then the ray parameter p equals $1/v_c$, where v_c is the critical refraction velocity. The angle $\eta(z)$ that the raypath makes with the vertical at any depth is then determined by a velocity ratio: $\eta(z) = \sin^{-1}[pv_i(z)] = \sin^{-1}[v_i(z)/v_c]$. Using this result, equations (A1) and (A2) reduce to

$$\Delta t_i = \frac{1}{a_i}\ln\left[\frac{(1+\cos\eta_i)\sin\eta_i'}{(1+\cos\eta_i')\sin\eta_i}\right], \tag{A3}$$

and

$$\Delta x_i = \frac{v_c}{a_i}\left[\cos\eta_i - \cos\eta_i'\right], \tag{A4}$$

where $\eta_i = \sin^{-1}(v_i/v_c)$ and $\eta_i' = \sin^{-1}(v_i'/v_c)$. η_i and η_i' are the incident angles of the circular raypath segment at the top and bottom of layer i, respectively.

The refraction delay time contribution of the i^{th} layer is defined as

$$\Delta\tau_i = \Delta t_i - \frac{\Delta x_i}{v_c} \quad . \tag{A5}$$

Substituting from equations (A3) and (A4) yields

$$\Delta\tau_i = \frac{1}{a_i}\ln\left[\frac{Q_i}{Q_i'}\right], \tag{A6}$$

where quantities Q_i and Q_i' are given by

$$Q_i = \frac{1+\cos\eta_i}{\sin\eta_i \exp(\cos\eta_i)}, \qquad Q_i' = \frac{1+\cos\eta_i'}{\sin\eta_i' \exp(\cos\eta_i')}. \tag{A7a,b}$$

As a check on the correctness of this result, examine the case where the vertical velocity gradient of the layer vanishes ($a_i \to 0$). In this situation, the raypath becomes a straight line segment, and the angles η_i and η_i' both approach the same angle $\eta_0 = \sin^{-1}[v_i(0)/v_c]$. Application of L'Hopital's rule to equation (A6) then yields

$$\lim_{a_i \to 0} \Delta\tau_i = \frac{(z_{i+1} - z_i)\cos\eta_0}{v_i(0)} = \frac{h_i \cos\eta_0}{v_i(0)}.$$

This is the proper expression for the one-way delay time contribution of a layer with thickness h_i and uniform velocity $v_i(0)$.

The one-way refraction delay time associated with a stack of n horizontal layers is obtained by summing expression (A6):

$$\Delta\tau = \sum_{i=1}^{n} \Delta\tau_i = \sum_{i=1}^{n} \frac{1}{a_i}\ln\left[\frac{Q_i}{Q_i'}\right]. \tag{A8}$$

This formula naturally accommodates any velocity discontinuities at the interfaces (i.e., $v'_{i-1} \neq v_i$). However, if the velocity function is continuous between all layers (as in the PRA example) then $Q_i' = Q_{i+1}$ and expression (A8) simplifies to

$$\Delta\tau = \sum_{i=1}^{n} \frac{1}{a_i} \ln\left[\frac{Q_i}{Q_{i+1}}\right]. \qquad \text{(A9)}$$

The static correction applied to the picked arrival times is designed to remove the one-way refraction delay time influence of the layered near surface structure, and add the delay time associated with a uniform replacement medium of equal thickness. If the replacement velocity is designated v_r, then the static shift is

$$t_{static} = -\Delta\tau + \frac{\cos\eta_r}{v_r} \sum_{i=1}^{n} h_i \,, \qquad \text{(A10)}$$

where $\eta_r = \sin^{-1}(v_r/v_c)$. Although this formula has been derived within the context of upward wave propagation through a set of horizontal layers, it also applies to the downward propagation portion of the total raypath. Hence, it may be used for the computation of either a source site static or a receiver site static.

Near surface velocity information along lines A and B of the PRA experiment are obtained from models developed by Zelt (1989, p. 40) from well logs. There are eight wells along line A and seven wells along line B. At each wellsite, the velocity model is approximated by a 1D stack of layers with linear velocities, and a static correction is calculated via formula (A10). The critical and replacement velocities are assumed to be v_c = 8.25 km/s and v_r = 6.6 km/s, respectively. These wellsite static corrections are then interpolated/extrapolated to the receiver locations along each line using the following procedure. First, a straight line is fitted to the coordinates of all recording stations and wellsites along a profile using the York algorithm (York 1966). This algorithm minimizes the sum of the squared deviations of the points measured perpendicular to the fitted straight line. The coordinates of these projected points are automatically returned by the algorithm. Finally, the wellsite statics are linearly interpolated/extrapolated in these projected coordinates to the receiver sites. Figure A1a displays the computed receiver static corrections for both lines; squares denote the wellsite statics calculated from expression (A10). The magnitudes of the statics are approximately the same on both lines (~300 ms), although there is a noticeable increase toward the southern end of line A.

The static corrections calculated with the above procedure apply only to receiver sites. However, since shot A4 is located at the end of profile B, a source static is readily estimated for this shot from the nearest

computed receiver correction (-290 ms). A source static for the isolated shot B4 must be assumed; the value adopted here is -300 ms.

Figure A1b depicts receiver static corrections recalculated with replacement and critical velocities equal to 6.2 km/s and 8.5 km/s, respectively. These velocity values are consistent with layer and halfspace velocities obtained from the 3D inversion procedure. Trends and magnitudes are similar. Source statics associated with these new receiver statics are assumed to be –210 ms for shot A4 and –250 ms for shot B4.

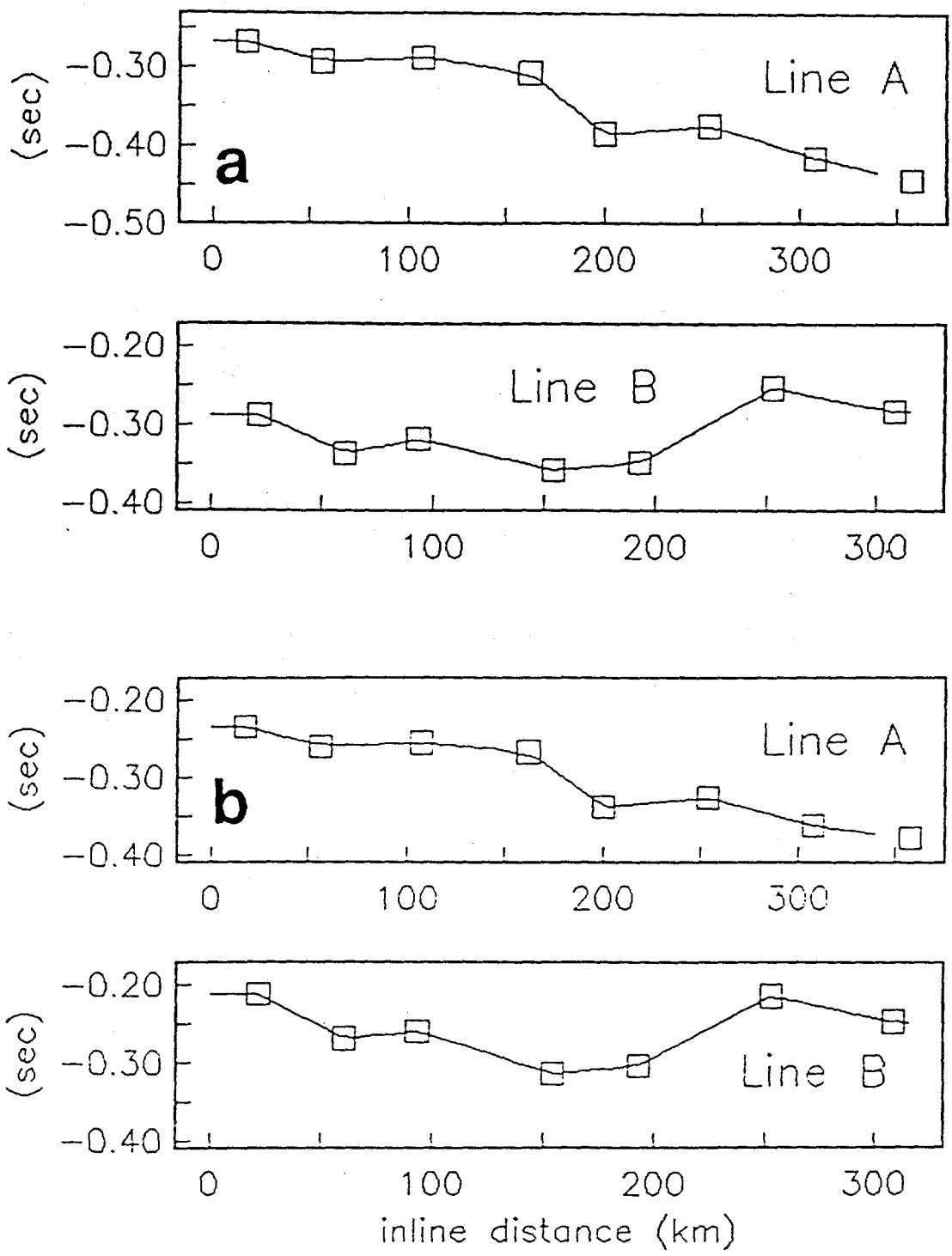
(sec)
−0.30
−0.40
−0.50
a
Line A
0
100
200
300
(sec)
−0.20
−0.30
−0.40
Line B
0
100
200
300
(sec)
−0.20
−0.30
−0.40
b
Line A
0
100
200
300
(sec)
−0.20
−0.30
−0.40
Line B
0
100
200
300
inline distance (km)

Fig. A1